Research Square

Preprints are preliminary reports that have not undergone peer review.
They should not be considered conclusive, used to inform clinical practice,
or referenced by the media as validated information.

Landslide Susceptibility Mapping through the Integration of Pixel and Slope Unit Analyses: A Case Study in El Salvador, Central America

Christian Conoscenti
University of Palermo: Universita degli Studi di Palermo
Abel Alexei Argueta-Platero
University of El Salvador: Universidad de El Salvador
Liborio Barbera
University of Palermo: Universita degli Studi di Palermo
Chiara Martinello
chiara.martinello@unipa.it

Universita degli Studi di Palermo https://orcid.org/0000-0001-9527-487X
Claudio Mercurio
University of Palermo: Universidad de Palermo
Edoardo Rotigliano
University of Palermo: Universidad de Palermo

Research Article

Keywords: Landslide susceptibility, Slope units, Tropical storm, Multivariate Adaptive Regression Splines (MARS), Random Forest, Ilopango Caldera (El Salvador)

Posted Date: June 4th, 2026

DOI: https://doi.org/10.21203/rs.3.rs-9403172/v1

License: This work is licensed under a Creative Commons Attribution 4.0 International License.
Read Full License

Landslide Susceptibility Mapping through the Integration of Pixel and Slope Unit Analyses: A Case Study in El Salvador, Central America

Christian Conoscenti[a], Abel Alexei Argueta-Platero[a,b], Liborio Barbera[a], Chiara Martinello[a*], Claudio Mercurio[a], Edoardo Rotigliano[a]

[a]Dipartimento di Scienze della Terra e del Mare (DiSTeM), University of Palermo, Via Archirafi 22, 90123 Palermo, Italy
[b]Escuela de Posgrado y Educación Continua, Facultad de Ciencias Agronómicas, University of El Salvador, Final de Av. Mártires y Héroes del 30 Julio, San Salvador 1101, El Salvador

*Correspondence to: Chiara Martinello; e-mail: chiara.martinello@unipa.it

Abstract

Landslide susceptibility mapping is commonly performed using either pixel-based or slope-unit (SU)-based approaches, each characterised by specific advantages and limitations. In this study, SU-level information is incorporated directly into a pixel-based modelling framework to assess whether this integration improves model performance and the spatial organisation of susceptibility maps. The analysis focuses on the northern sector of the Ilopango Caldera (El Salvador), where shallow landslides were triggered by Tropical Storms Amanda and Cristobal in 2020. A 2 m resolution LiDAR-derived DEM was used to derive pixel-scale terrain predictors and to delineate slope units through hydrological analysis.

Two configurations were tested: a Baseline model based solely on pixel-scale variables and an Enhanced model including SU-based morphometric summaries and lithological proportions. Both configurations were implemented using Multivariate Adaptive Regression Splines (MARS) and Random Forest (RF) and evaluated through repeated spatial cross-validation.

The Enhanced models systematically outperformed the Baseline models. Mean AUC increased from 0.927 to 0.942 for MARS and from 0.923 to 0.949 for RF. In addition to the improvement in predictive performance, the Enhanced configuration produced maps characterised by higher spatial autocorrelation, measured using Global Moran's I, and reduced local fragmentation, while maintaining variability within individual slope units.

These results indicate that integrating SU-derived descriptors during model calibration strengthens the predictive capability of pixel-based models and improves the spatial consistency of the resulting maps, without sacrificing pixel-scale detail.

Keywords: Landslide susceptibility; Slope units; Tropical storm; Multivariate Adaptive Regression Splines (MARS); Random Forest; Ilopango Caldera (El Salvador)

1 Introduction

Landslides represent a recurrent and often destructive process in many tropical regions, where steep terrain and intense rainfall create conditions favourable to slope instability. In Central America, and particularly in El Salvador, these factors are compounded by the widespread presence of weak volcanic deposits, including the Tierra Blanca Joven (TBJ) tephra, which mantles large portions of the landscape. Under dry conditions, these deposits may appear relatively stable, yet their shear strength decreases rapidly when saturated, favouring shallow failures during high-intensity rainfall events.

In recent decades, several severe rainfall-triggered landslide events have affected the country, producing casualties and extensive damage to infrastructure. Among the most significant was Hurricane Ida in 2009, which triggered widespread slope failures across central El Salvador (Rotigliano et al. 2019; Mercurio et al. 2021), highlighting the extreme sensitivity of the volcanic slopes to short-duration, high-intensity rainfall. More recently, Tropical Storms Amanda and Cristobal in 2020 generated thousands of slope failures across the northern sector of the Ilopango Caldera, highlighting once more the intrinsic fragility of the area.

Landslide susceptibility mapping (LSM) aims to identify areas where slope failures are more likely to occur, based on the assumption that future landslides will develop under environmental conditions similar to those that controlled past events (Carrara et al. 1995; Guzzetti et al. 2005). LSM commonly relies on statistical or machine learning techniques calibrated on landslide inventories and geo-environmental predictors derived from digital elevation models and thematic maps (Brenning 2005; Reichenbach et al. 2018). While considerable effort has been devoted to improving algorithms and validation strategies, the spatial reference framework over which susceptibility is estimated – the mapping unit – remains a critical but sometimes underestimated component of the modelling process.

Among the available mapping units in landslide susceptibility modelling, grid cells (pixels) and slope units are by far the most commonly adopted (Reichenbach et al. 2018). Pixel units, typically corresponding to the resolution of a DEM, allow detailed representation of local morphometric

variability and are well suited to capture conditions influencing landslide initiation. For this reason, many LSM studies rely on grid-based implementations (Vorpahl et al. 2012; Rotigliano et al. 2018; Vargas-Cuervo et al. 2019; Conoscenti et al. 2015). However, when applied at high spatial resolution, pixel-based models frequently generate highly fragmented patterns, with adjacent cells showing markedly different susceptibility values. This behaviour, often described as a "salt-and-pepper" effect, may complicate the interpretation and practical use of the resulting maps (Martinello et al. 2021, 2023).

Slope units (SUs), in contrast, represent morphologically coherent hillslope domains delimited by drainage divides and channel networks. SU-based approaches explicitly adopt hillslope partitions as modelling entities and are widely used in susceptibility assessments where geomorphological coherence is prioritised (Rossi et al. 2010; Amato et al. 2023; Rolain et al. 2023; Martinello et al. 2021). Nevertheless, SU-based modelling may obscure intra-slope variability, and its performance depends strongly on how the units are delineated. Previous studies have shown that the selection of the mapping unit affects not only predictive performance but also the spatial structure of susceptibility maps (Jacobs et al. 2020; Canavesi et al. 2020; Alvioli et al. 2020).

Despite this awareness, most applications adopt either pixel-based or SU-based strategies. Attempts to integrate the two representations have generally involved post-processing of pixel-based susceptibility maps through aggregation or restructuring within slope units, often resulting in outputs that are expressed at the SU level (Van Den Eeckhaut et al. 2009; Domènech et al. 2020; Martinello et al. 2021, 2022a). While these approaches may enhance spatial coherence, they typically modify the cartographic representation rather than the calibration framework itself.

In this study, we adopt a multiscale statistical approach in which slope-unit information is incorporated directly into a pixel-based modelling framework. A Baseline configuration relies solely on pixel-scale predictors, whereas an Enhanced configuration includes additional descriptors derived at the SU scale, such as summary statistics of morphometric variables and lithological proportions. Both configurations are implemented using Multivariate Adaptive Regression Splines (MARS) and Random Forest (RF), two algorithms that have been widely applied to model different geomorphic processes, including landslide and gully susceptibility, and have demonstrated robust predictive capability across different geomorphological contexts (e.g., Felicísimo et al. 2013; Youssef et al. 2016; Rotigliano et al. 2019; Martinello et al. 2022b; Conoscenti and Sheshukov 2023; Conoscenti et al. 2025). The main objective is to improve the predictive performance of pixel-based susceptibility models by integrating SU-level descriptors during model calibration. In doing so, we also evaluate whether this integration produces maps that are more spatially coherent, with reduced local fragmentation and clearer correspondence with hillslope organisation, while preserving pixel-scale detail and increasing their practical usefulness for land-use planners and policy makers.

2 Study Area

The study area is located in the northern sector of the Ilopango Caldera, El Salvador, and covers approximately 27 km² (Fig. 1). It includes the Arenal San Martín and Río Guluchapa catchments, together with smaller sub-basins draining toward Lake Ilopango. The area forms part of the Central American Volcanic Arc, where active tectonics and explosive volcanism have shaped a rugged and highly dissected landscape.

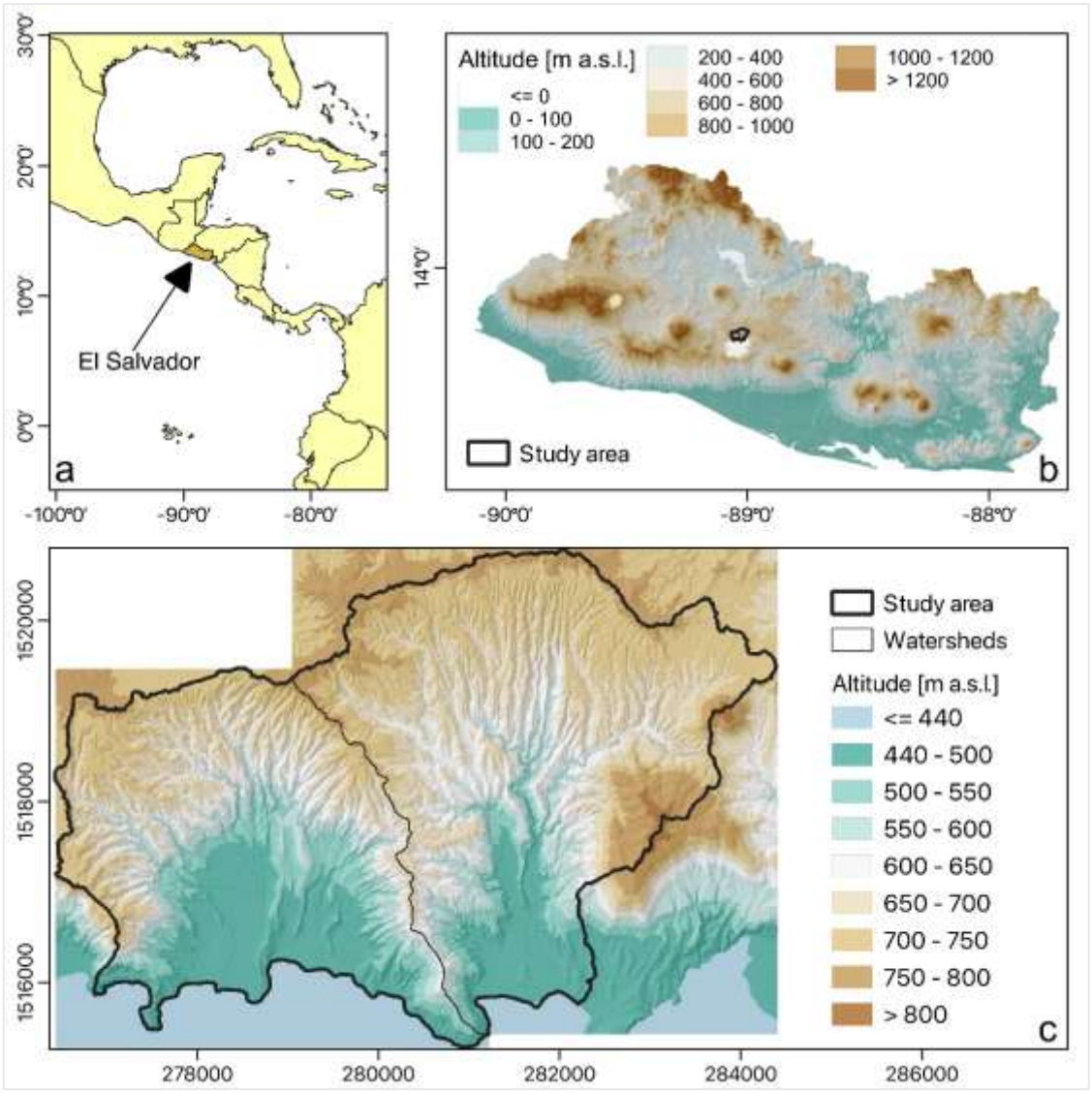


Fig. 1. Location of the study area: (a) the geographic position of El Salvador within Central America; (b) digital elevation model of El Salvador highlighting the Ilopango Caldera; (c) detailed view of the northern sector of the Ilopango Caldera showing the boundaries of the study area and the main watersheds.

Surface geology is dominated by deposits of the Tierra Blanca Joven eruption, consisting of unconsolidated dacitic to rhyolitic tephra, ignimbrites and ash layers (Fig. 2). These materials are highly porous and susceptible to rapid infiltration. When saturated, they may fail along shallow discontinuities, generating soil slips and debris flows. The morphology reflects both lithological weakness and structural control, with steep slopes, narrow valleys and deeply incised drainage networks.

The climate is tropical with a marked wet season extending from May to October. During this period, high-intensity rainfall events associated with tropical storms and hurricanes frequently occur. The northern sector of the Ilopango Caldera has been repeatedly affected by rainfall-triggered slope failures associated with major tropical events, including Hurricane Ida in 2009, Tropical Storms Amanda and Cristobal in 2020, and Hurricane Julia in 2022. The landslide inventory used in this study refers specifically to the shallow failures triggered by Amanda and Cristobal between late May and early June 2020, which produced prolonged rainfall leading to widespread soil saturation and slope instability, particularly on the northern flanks of the caldera.

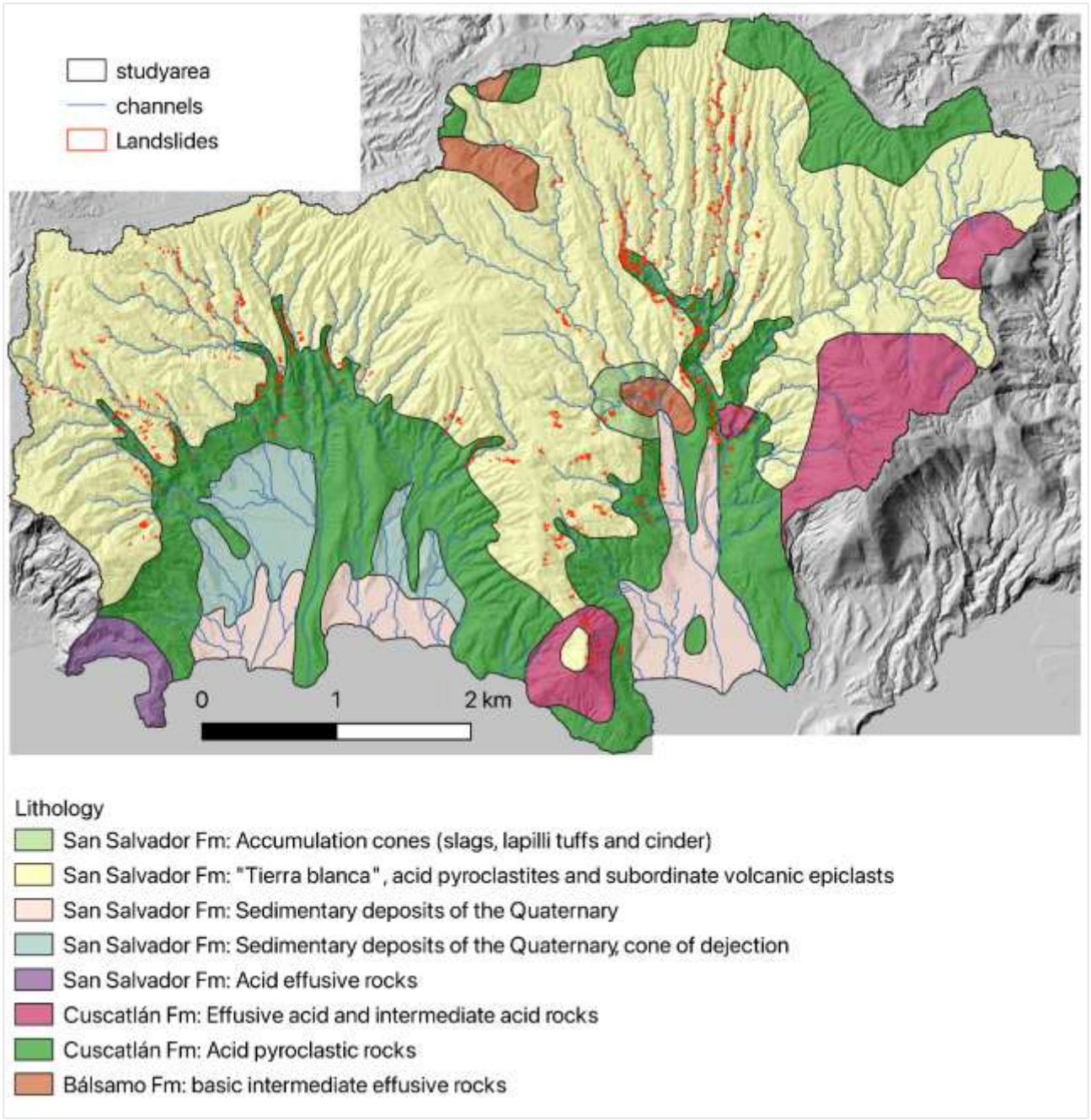


Fig. 2. Landslide inventory and lithological setting of the study area: distribution of landslides triggered by Tropical Storms Amanda and Cristobal over the main lithological units. Geological framework and landslide inventory after Argueta-Platero (2023).

3 Materials and Methods

Landslide susceptibility was modelled by integrating pixel-scale terrain predictors with slope-unit descriptors, including morphometric summaries and lithological proportions computed within each SU. All processing and analyses were performed in R (R Core Team 2023), primarily using the packages terra, dplyr, earth, randomForest, groupdata2, and caret, with terrain operations carried out through WhiteboxTools (Lindsay 2016).

3.1 Topographic Data and Landslide Inventory

Landslide susceptibility modelling was based on a 2 m resolution LiDAR-derived Digital Elevation Model (DEM), provided by the Ministry of Environment and Natural Resources (MARN) to the University of El Salvador (UES). The DEM was used as the reference topographic surface for deriving the geo-environmental predictors and for delineating the adopted mapping units.

Prior to terrain analysis, the DEM was hydrologically conditioned to remove spurious depressions using the Wang and Liu (2006) algorithm implemented in WhiteboxTools. Flow direction and flow accumulation grids were subsequently computed using the D8 algorithm (O'Callaghan and Mark 1984).

The landslide inventory includes 1,849 shallow landslides triggered by Tropical Storms Amanda and Cristobal (29 May - 7 June 2020). The inventory was compiled within the framework of the doctoral research by Argueta-Platero (2023). Landslides were mapped as polygons through visual interpretation of high-resolution Google Earth imagery acquired on 20 June 2020, shortly after the rainfall events. The post-event image shows clear areas of vegetation removal and exposed soil surfaces, particularly when compared with the pre-event image available for 7 November 2019.

To specifically characterize the slope failure initiation conditions and avoid introducing morphological signatures related to transport or depositional processes, a strict sampling strategy was applied (Fig. 3): (i) for each landslide polygon, the pixel with maximum elevation was identified and labelled as landslide initiation point (Presence = 1); (ii) the remaining pixels within landslide boundaries were excluded from the analysis; (iii) pixels outside mapped landslides were considered stable (Absence = 0) and were sampled within each cross-validation split to match the number of presence pixels. Pixels belonging to the drainage network were not included in the analysis, as they were not assigned to any SU and were therefore removed during the data cleaning step.

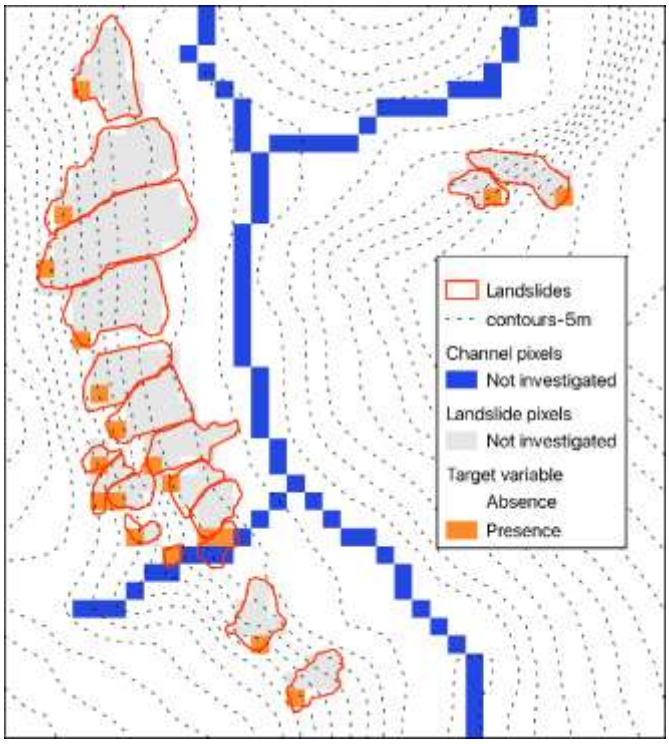


Fig. 3. Sampling strategy adopted to define the target variable: for each landslide polygon, the pixel with maximum elevation is selected as the initiation point (Presence = 1). The remaining pixels within the landslide body are excluded from the analysis (Not investigated) to avoid modelling transport and deposition zones. Pixels outside mapped landslides are considered stable (Absence = 0). Pixels belonging to the drainage network are not included in the analysis.

3.2 Geo-environmental Predictors and Mapping Units

Two predictor configurations were considered: a Baseline configuration based on pixel-scale variables and an Enhanced configuration including slope-unit (SU) descriptors (Table 1).
Pixel-scale predictors were derived from the DEM and processed in R. The selected variables include elevation (ELE), slope angle (SLO), aspect expressed as northness (N) and eastness (E), topographic wetness index (TWI), length-slope factor (LSF), relative position index (RPI), downslope distance to stream (DTS), elevation percentile (EPE), and lithology (GEO). Lithology was derived from the available geological map (Argueta-Platero 2023, and references therein) and treated as a categorical predictor. A representative sector of the study area showing the nine pixel-scale topographic predictors derived from the DEM is presented in Fig. 4.

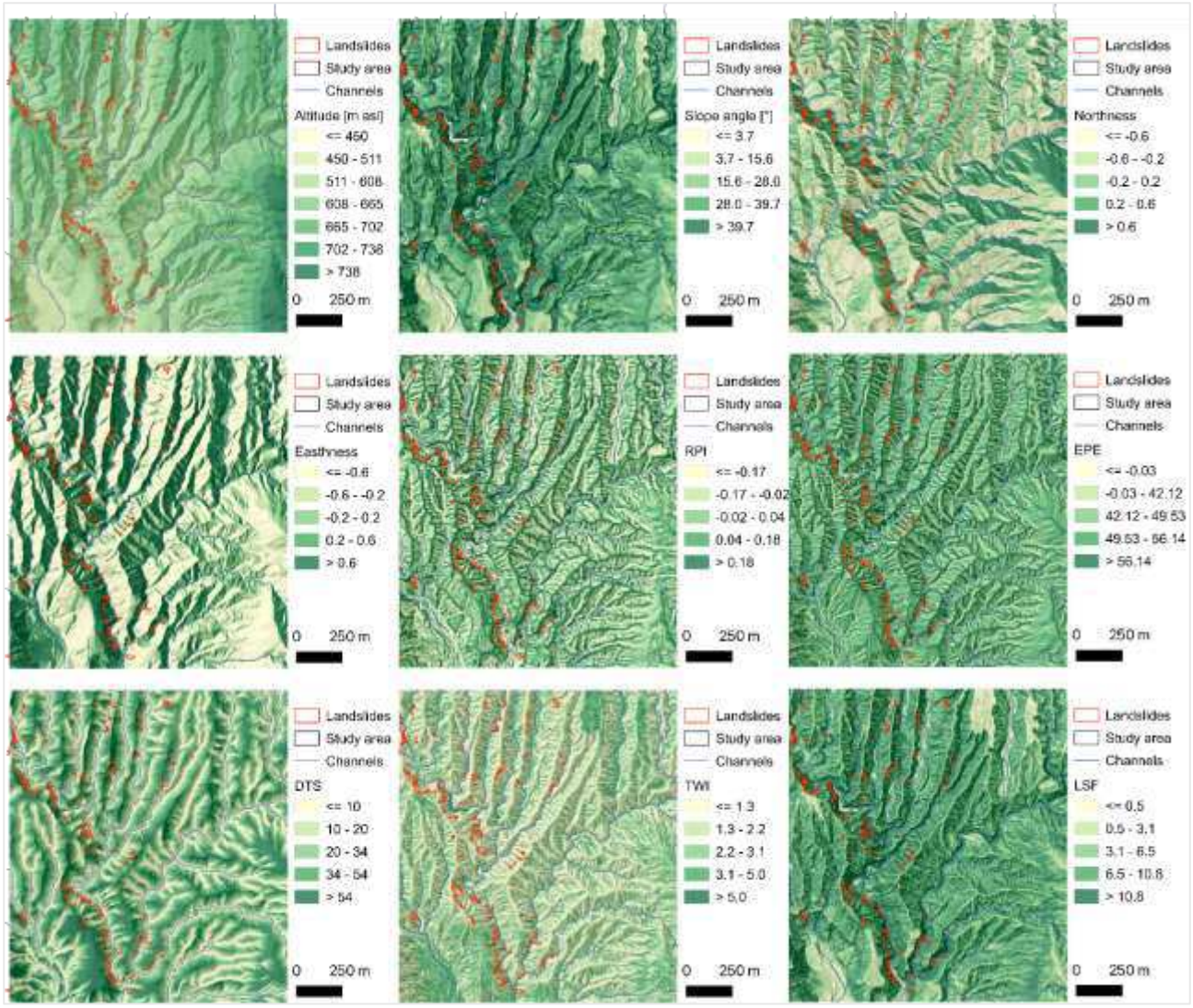


Fig. 5. Pixel-scale geo-environmental predictors derived from the 2 m DEM for a representative sector of the study area. From left to right and top to bottom: elevation (ELE), slope angle (SLO), northness (N), eastness (E), relative position index (RPI), elevation percentile (EPE), downslope distance to stream (DTS), topographic wetness index (TWI), and length–slope factor (LSF). Landslide polygons and channel network are overlaid for reference.

The topographic wetness index (TWI) was derived from a specific contributing area and slope. To reduce high-frequency variability associated with the 2 m resolution, a Gaussian filter ($\sigma = 2$) was subsequently applied, and the filtered TWI layer was used in the modelling. Aspect was transformed into sine and cosine components prior to modelling.

Slope Units were delineated through hydrological terrain analysis. A drainage network was extracted from the D8 flow accumulation grid using a contributing area threshold of 400 cells (approximately 1,600 m²). The threshold was selected to represent the fine-scale dissection of the study area and to obtain slope units consistent with the observed scale of slope failures, while avoiding excessive terrain fragmentation. Hillslopes were subsequently derived from the D8 flow pointer and the extracted stream network. In this framework, pixel units correspond to the 2 m × 2 m cells of the DEM, which constitute the fundamental spatial entities for modelling and for the extraction of terrain attributes. The relationship between pixel units and slope units within the study area is illustrated in Fig. 5.
For the Enhanced configuration, SU-level descriptors were derived from the pixel-based predictors. For each continuous variable, mean, standard deviation, 10th percentile and 90th percentile were computed within each SU and assigned back to the pixels belonging to that unit. Lithology was also represented at the SU scale by computing, for each unit, the proportion of the different geological classes. Eight variables were generated, each corresponding to the proportion of a specific lithological class within the unit.

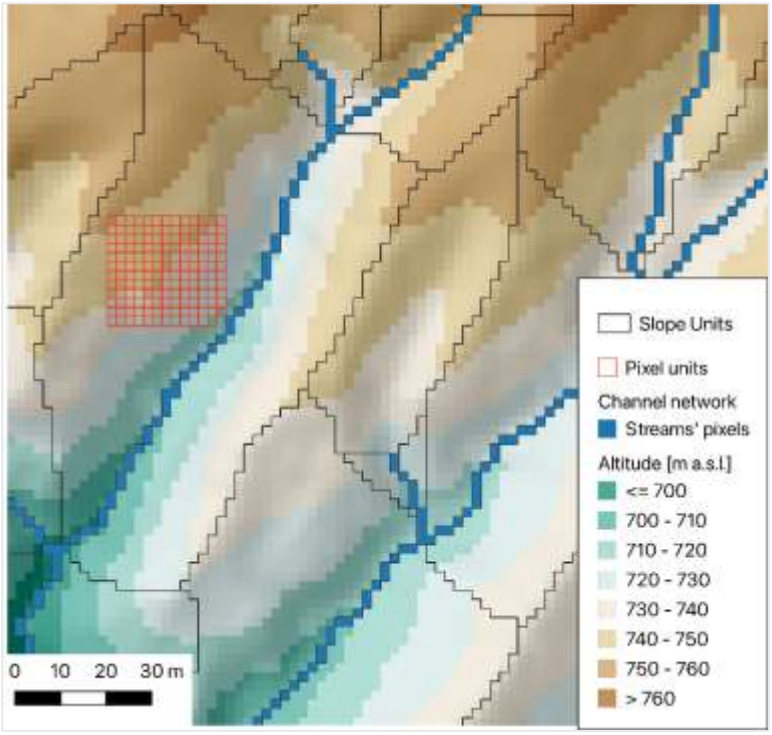


Fig 5. Spatial relationship between pixel units and slope units (SUs) within the study area.

Multicollinearity was assessed on the complete set of continuous predictors, including SU-based descriptors, using a Pearson correlation matrix. Variables exhibiting absolute correlation coefficients |r| greater than 0.7 were identified using *findCorrelation()* (Kuhn 2008) and excluded from the modelling dataset. Three pixel-scale variables (N, E and EPE) were removed as a result of the multicollinearity analysis. In addition, 23 out of the 45 SU-based statistical descriptors were excluded from the modelling dataset.

Table 1. Predictors used in the Baseline and Enhanced configurations.

Variable	Description	Scale	Baseline	Enhanced
ELE	Elevation (m)	Pixel	✓	✓
SLO	Slope angle (°)	Pixel	✓	✓
N, E	Northness and Eastness	Pixel	✓	✓

Variable	Description	Scale	Baseline	Enhanced
TWI	Gaussian-smoothed Topographic Wetness Index	Pixel	✓	✓
LSF	Length–Slope factor	Pixel	✓	✓
RPI	Relative Position Index	Pixel	✓	✓
DTS	Downslope distance to stream	Pixel	✓	✓
EPE	Elevation percentile	Pixel	✓	✓
GEO	Lithological class (factor)	Pixel	✓	✓
SU statistics	Mean, SD, Q10, Q90 of continuous predictors	SU	–	✓
GEO_i_prop	Proportion of lithological classes within the SU	SU	–	✓

3.3 Machine Learning Models

Landslide susceptibility was modelled using Multivariate Adaptive Regression Splines (MARS) and Random Forest (RF).
MARS models the relationship between the response and the predictors through piecewise linear basis functions (Friedman 1991). The predictor space is partitioned by introducing knots where changes in the response-predictor relationship occur, and relevant terms are retained through a forward selection followed by backward pruning. In this study, MARS was implemented in R using a binomial formulation to estimate landslide occurrence probability. The models were fitted considering additive terms only (degree = 1).
Random Forest (Breiman 2001) builds an ensemble of classification trees grown on bootstrap samples of the training data. At each node, a random subset of predictors is evaluated, and the best split is selected. Predictions are obtained by aggregating the trees. RF models were fitted with 500 trees (ntree = 500) and mtry = 3.
Both algorithms were applied under the Baseline and Enhanced predictor configurations described above.

3.4 Spatial cross-validation and performance assessment

To reduce spatial dependence between training and validation data, a spatial cross-validation strategy was adopted (Fig. 6). The study area was partitioned into 125 square tiles of 500 m side length (0.25 km²). Tiles were assigned to five folds using the groupdata2 package. The 5-fold procedure was repeated five times, resulting in 25 model runs for each configuration.
Within each fold, presence and absence pixels were balanced prior to model fitting.
Model performance was evaluated using Area Under the Receiver Operating Characteristic Curve (AUC) and Cohen's Kappa (κ), computed using a probability threshold of 0.5. Differences between Baseline and Enhanced configurations were tested using the Wilcoxon signed-rank test (paired, one-sided).

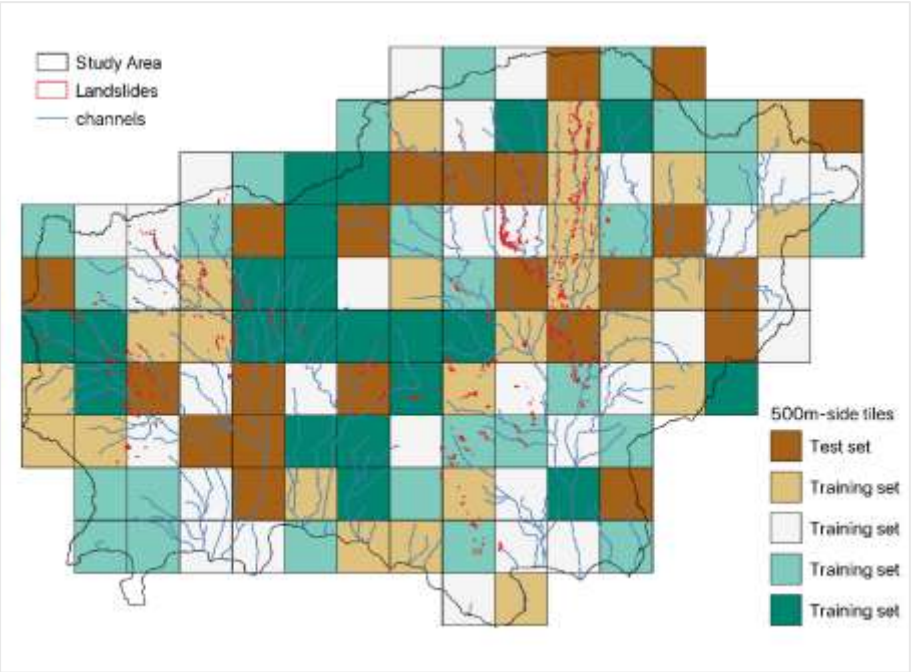


Fig. 6. Spatial cross-validation scheme based on 500 m tiles.

3.5 Susceptibility mapping and map evaluation

After cross-validation, the four model configurations were recalibrated using the complete dataset (excluding landslide body and drainage pixels) and subsequently applied to the entire study area to generate continuous probability maps of landslide occurrence.
Model performance at map scale was further assessed through success rate curves. Predicted probabilities were ranked in descending order, and cumulative percentages of landslide initiation pixels were plotted against cumulative percentages of the study area. The area under the success rate curve was computed as an additional measure of model goodness-of-fit.
The spatial structure of the susceptibility maps was evaluated using Global Moran's I, calculated on the predicted probability values. The index was used to quantify spatial autocorrelation and to compare the spatial structure of the Baseline and Enhanced configurations.

4. Results

4.1 Cross-validation performance

The spatial cross-validation procedure produced 25 model runs for each of the four configurations (MARS–Baseline, MARS–Enhanced, RF–Baseline, RF–Enhanced), AUC and Cohen's κ were computed for all runs.
Enhanced configurations systematically outperformed Baseline configurations for both algorithms (Fig. 7). MARS mean AUC values increased from 0.927 (SD = 0.016) in the Baseline configuration to 0.942 (SD = 0.018) in the Enhanced configuration. Accordingly, RF mean AUC increased from 0.923 (SD = 0.019) to 0.949 (SD = 0.018). Similar improvements were observed for Cohen's κ, with mean values increasing from 0.710 to 0.741 for MARS and from 0.707 to 0.741 for RF.

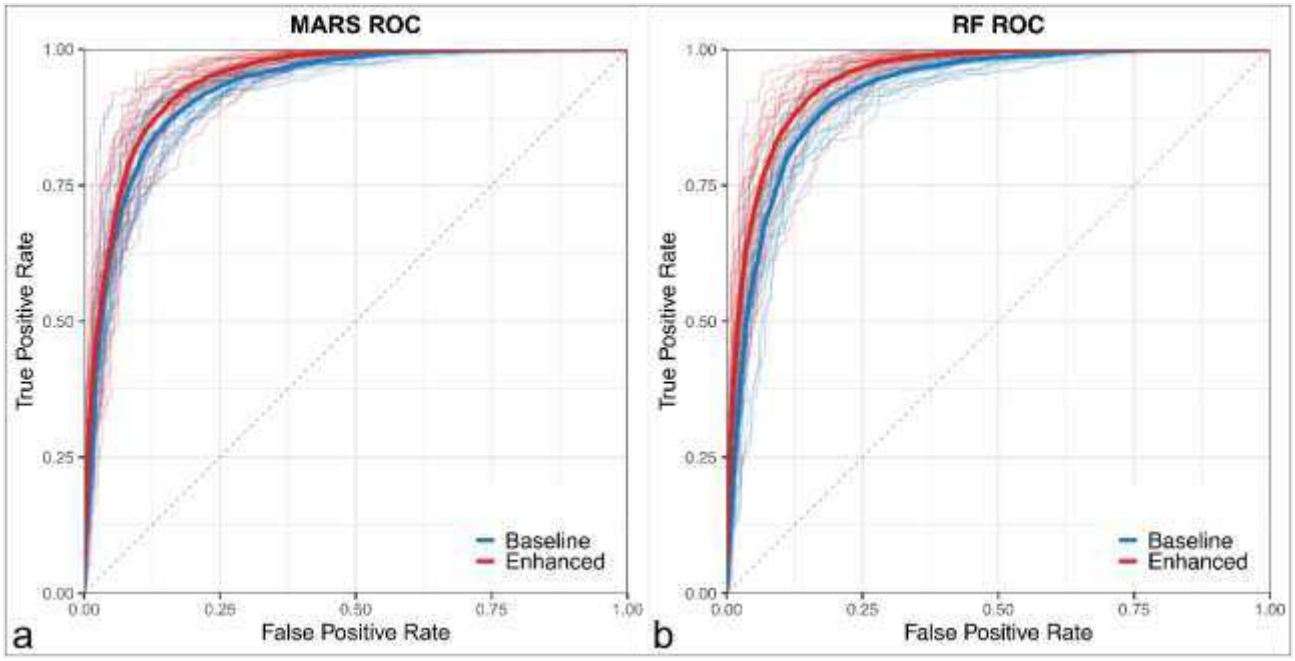


Fig. 7. Receiver Operating Characteristic (ROC) curves for (a) MARS and (b) Random Forest under Baseline and Enhanced configurations.

The distribution of AUC and κ values across runs is shown in Fig. 8. Enhanced configurations display higher median values and, for AUC, slightly reduced interquartile range compared to Baseline configurations.

Wilcoxon signed-rank tests indicate that the improvement in both AUC and κ between Baseline and Enhanced configurations is statistically significant for the two algorithms ($p < 0.01$).

Between algorithms, a statistically significant difference was observed only for AUC in the Enhanced configuration, where RF outperformed MARS. For the remaining comparisons, including Cohen's κ in both configurations and AUC in the Baseline configuration, differences between MARS and RF were not statistically significant.

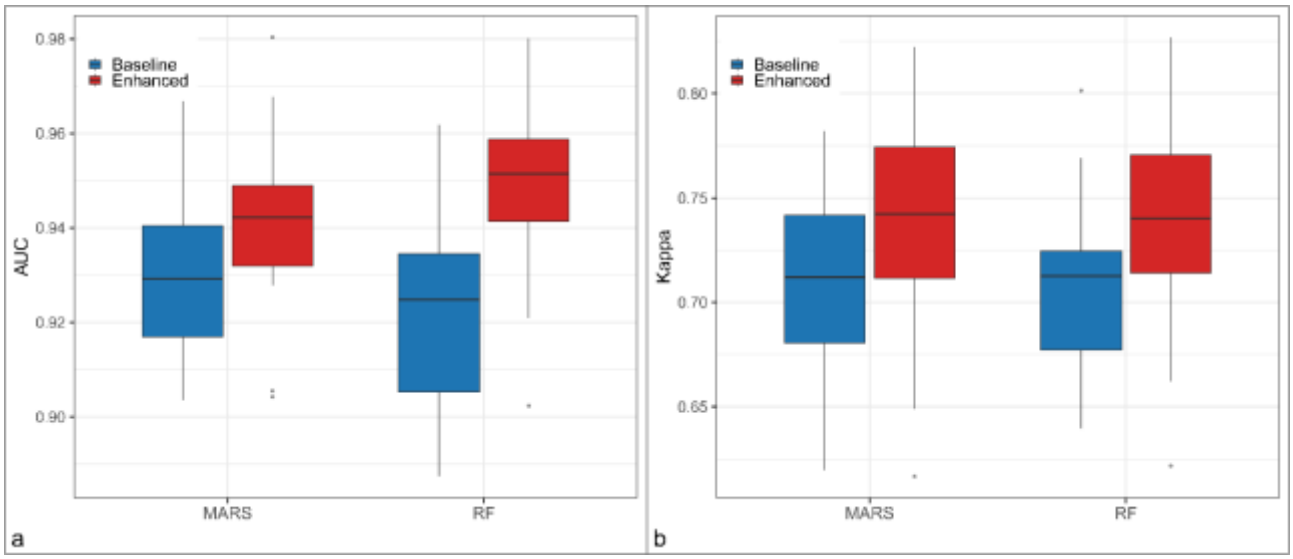


Fig. 8. Distribution of (a) AUC and (b) Cohen's κ values obtained from the 25 repeated spatial cross-validation runs for the Baseline and Enhanced configurations.

4.2 Susceptibility maps and success rate analysis

The susceptibility maps obtained from the four model configurations are shown in Fig. 9. For clarity, a representative portion of the study area is displayed, as the full extent would not allow a detailed visual comparison. High predicted probabilities are mainly concentrated on steeper hillslopes. This pattern is supported by the strong positive correlation between predicted scores and slope (Spearman's ρ ranging from 0.64 to 0.80 across configurations, $p < 0.001$), indicating a marked topographic gradient in model response.

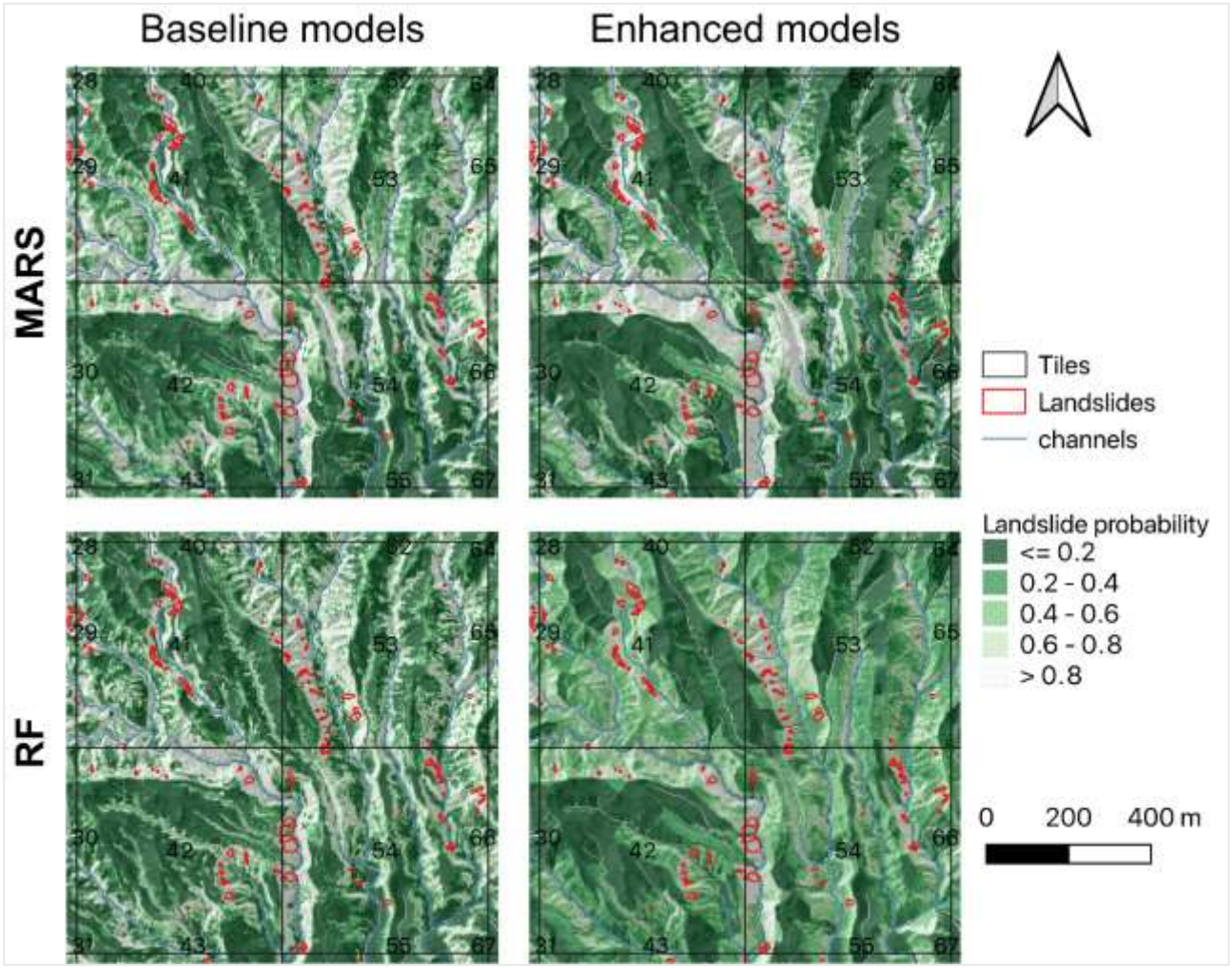


Fig. 9. Susceptibility maps obtained from the four model configurations for a representative portion of the study area.

At broader scale, susceptibility patterns are also influenced by lithological distribution. Landslides are predominantly located within the Tierra Blanca unit (74% of the inventory) and within the acidic pyroclastic rocks of the Cuscatlán Formation (22%), which cover 56% and 25% of the study area, respectively. This indicates a non-uniform distribution of failures across lithological classes. Accordingly, elevated susceptibility values are mainly associated with these units, although slope remains the primary discriminating factor at the hillslope scale.

Model performance at map scale was evaluated using success rate curves (Fig. 10). Enhanced configurations capture a larger proportion of landslide initiation pixels within the highest-ranked areas compared to Baseline configurations. The area under the success rate curve confirms this trend: for MARS, it increases from 0.885 in the Baseline configuration to 0.915 in the Enhanced configuration, whereas for RF it increases from 0.898 to 0.943. The RF–Enhanced configuration achieves the highest cumulative capture of landslides within limited portions of the study area.

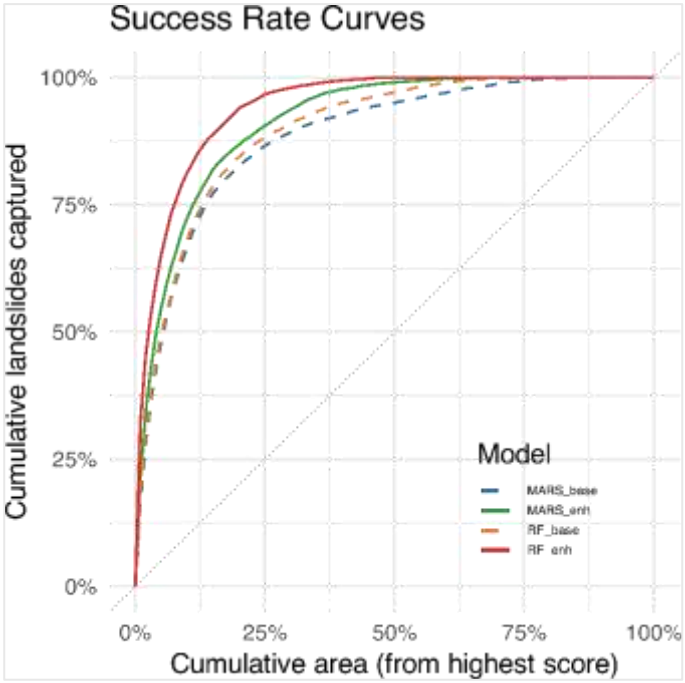


Fig. 10. Success rate curves for Baseline and Enhanced configurations.

4.3 Spatial structure of susceptibility maps

Global Moran's I values computed on the final probability maps indicate clear differences in spatial structure between configurations. For MARS, Moran's I increased from 0.930 in the Baseline configuration to 0.947 in the Enhanced configuration. For RF, the increase was more pronounced, from 0.891 to 0.962. All values were statistically significant according to permutation tests ($p = 0.004$), computed on an aggregated grid to reduce local-scale noise.

Fig. 11 provides a zoomed view of the same portion of the study area shown in Fig. 9, allowing a clearer comparison of the spatial structure of the four maps. The visual comparison supports these results. In the Enhanced configurations, predicted probabilities show greater internal consistency within individual SUs, resulting in a more homogeneous hillslope-scale pattern. Probability values are not uniform within each SU, as would be the case in models calibrated directly at SU level; however, the Enhanced maps reflect SU boundaries more clearly and exhibit fewer isolated high-score pixels.

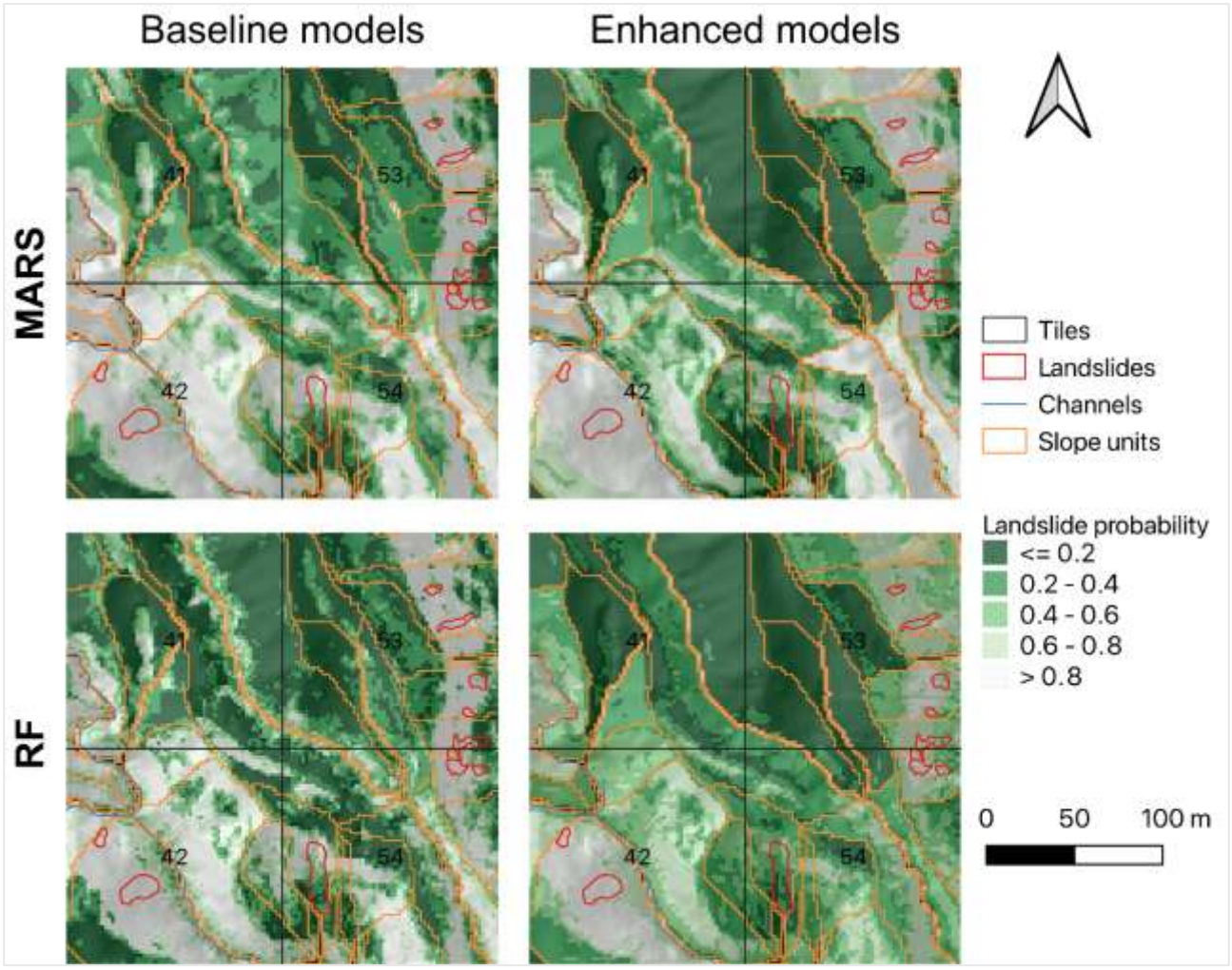


Fig. 11. Zoomed view of the area shown in Fig. 9 highlighting differences in spatial structure between Baseline and Enhanced configurations and their relationship with slope units.

5. Discussion

The results confirm that mapping unit choice influences both predictive performance and spatial structure. While the Baseline configuration already achieves high discrimination capacity, the integration of SU-level descriptors systematically improves AUC, κ, and success rate metrics.

Previous studies have demonstrated that mapping unit selection substantially affects the spatial structure and interpretation of susceptibility outputs (Van Den Eeckhaut et al. 2009; Domènech et al. 2020). Van Den Eeckhaut et al. (2009) showed that grid-cell- and topographic-unit-based assessments may lead to markedly different zonations and proposed a heuristic combination of the two approaches to improve the final map. Domènech et al. (2020), within a hazard-oriented framework, structured pixel-based susceptibility results by aggregating them within slope units to estimate failure magnitude and reduce internal fragmentation. In contrast, the Enhanced configuration proposed here integrates SU-scale descriptors directly during model calibration rather than restructuring pixel-based outputs a posteriori, allowing hillslope context to influence probability estimation while preserving pixel resolution.

Recent research has shown that susceptibility patterns depend strongly on SU partitioning. Martinello et al. (2021) examined how different slope-unit partitions affect the spatial distribution of susceptibility results, showing that changes in unit geometry can modify both map structure and model response when pixel-based scores are aggregated within alternative SU schemes. In a subsequent study, Martinello et al. (2022a) explored landform-based slope units and showed that units derived from landform classification not only produce maps that are more consistent with

hillslope morphology than simple hydrological partitions but may also improve predictive performance under appropriate modelling strategies. In contrast, the approach adopted in this study does not dissolve or reassign pixel scores to predefined slope units but integrates SU-derived descriptors directly into the calibration phase, allowing hillslope-scale information to influence the estimation of pixel-level probabilities while maintaining full spatial resolution.

In the present study, a single hydrologically derived SU partition was adopted, calibrated to reflect the fine-scale dissection of the study area and the spatial extent of observed failures. This choice was intended to ensure that slope units remained comparable in scale to the dominant shallow landslides observed in the inventory, thereby avoiding excessive aggregation of geomorphologically distinct sectors. The increase in Global Moran's I observed for the Enhanced configurations indicates that this partition contributes to reducing high-frequency spatial variability while maintaining intra-unit gradients. In other words, the SU framework acts as a structural constraint that moderates pixel-scale fragmentation without suppressing meaningful variability within individual hillslopes. Unlike optimisation-focused approaches, the present study adopts a SU partition tailored to the geomorphological characteristics of the study area, and the results indicate that this partition is sufficient to enhance spatial coherence within the proposed multiscale framework.

A strong topographic control on susceptibility is evident. Predicted scores are strongly correlated with slope across configurations, confirming that steepness dominates probability gradients at the hillslope scale. At broader scale, lithological distribution also influences susceptibility patterns. Landslides are predominantly located within the Tierra Blanca unit and the acidic pyroclastic rocks of the Cuscatlán Formation, indicating non-uniform distribution across lithological classes. The Enhanced configuration allows this lithological control to be incorporated without enforcing strict homogeneity within slope units.

The proposed multiscale framework represents a compromise between pixel-based and SU-based modelling. Pixel-only approaches may generate fragmented maps, especially at high spatial resolution, whereas pure SU-based approaches may oversimplify internal variability by assigning uniform values to morphologically complex hillslopes. By integrating SU-derived descriptors within a pixel-level calibration scheme, the Enhanced configuration reduces spatial fragmentation while preserving fine-scale variability linked to local morphometric and lithological contrasts. In this sense, the framework does not merely smooth the susceptibility surface but reorganises it according to hillslope structure without suppressing local gradients. Future investigations could explore the sensitivity of the proposed framework to alternative partitioning schemes and assess its transferability to different geomorphological contexts.

Overall, the integration of pixel- and slope- unit-scale information offers a structured and reproducible approach to improving both predictive performance and spatial organisation of susceptibility maps in highly dissected volcanic terrains.

6. Conclusions

This study evaluated the effect of integrating slope-unit descriptors within a pixel-based landslide susceptibility framework. The comparison between the Baseline and Enhanced configurations indicates that including SU-derived predictors improves model performance, as reflected by higher AUC, Cohen's κ, and success rate values.

In addition to these performance indicators, incorporating SU information alters the spatial arrangement of predicted probabilities, leading to maps with a clearer and more structured pattern. Enhanced configurations exhibit higher spatial autocorrelation and reduced fragmentation, while preserving local variability at the pixel scale. The results indicate that incorporating hillslope-scale context during model calibration represents a practical way to reduce high-frequency spatial noise without resorting to full aggregation at the slope-unit level.

The analysis also confirms the dominant role of slope in controlling susceptibility patterns at the hillslope scale, while lithological distribution influences the broader spatial organisation of predicted probabilities. The multiscale framework allows these controls to be represented simultaneously. Although the study relies on a single SU delineation scheme, the proposed methodology is flexible and can be adapted to alternative partitioning strategies. The approach may therefore provide a useful basis for susceptibility assessment in similar geomorphological settings where high-resolution DEMs and detailed inventories are available.

Acknowledgements

This research was funded by the Italian Agency for Development Cooperation (AICS) within the project "Establecer y desarrollar la carrera de Licenciatura en Ciencias de la Tierra con énfasis en Geología en la Universidad de El Salvador (CASTES)" (AID 11726). The scientific responsible of the project is Christian Conoscenti (University of Palermo).

CRediT author statement

Christian Conoscenti: Conceptualisation, Methodology, Formal analysis, Writing – original draft, Writing – review & editing, Supervision, Funding acquisition. **Chiara Martinello:** Conceptualisation, Methodology, Formal analysis, Writing – review & editing. **Abel Alexei Argueta-Platero:** Investigation, Data curation, Formal analysis, Writing – review & editing. **Claudio Mercurio:** Data curation, Formal analysis, Writing – review & editing. **Liborio Barbera:** Data curation, Formal analysis, Writing – review & editing. **Edoardo Rotigliano:** Conceptualisation, Supervision, Writing – review & editing.

References

Alvioli M, Guzzetti F, Marchesini I (2020) Parameter-free delineation of slope units and terrain subdivision of Italy. Geomorphology 358, 107124. https://doi.org/10.1016/j.geomorph.2020.107124

Amato G, Fiorucci M, Martino S, Lombardo L, Palombi L (2023) Earthquake-triggered landslide susceptibility in Italy by means of Artificial Neural Network. Bulletin of Engineering Geology and the Environment 82 (5), 160. https://doi.org/10.1007/s10064-023-03163-x

Argueta-Platero A (2023) MODELOS DE SUSCEPTIBILIDAD PARA FLUJOS DE DETRITOS ACTIVADOS POR EL EVENTO EXTREMO DE LLUVIA PRODUCTO DE LAS TORMENTAS TROPICALES EP022020/AMANDA Y AL032020/CRISTOBAL EN EL SALVADOR. PhD thesis, University of Palermo. Available at: https://iris.unipa.it/handle/10447/619854 (accessed 07 March 2026)

Breiman L. (2001) Random forests. Machine Learning, 45(1), 5–32. https://doi.org/10.1023/A:1010933404324

Brenning A (2005) Spatial prediction models for landslide hazards: review, comparison and evaluation. Natural Hazards and Earth System Sciences 5, 853–862. https://doi.org/10.5194/nhess-5-853-2005

Canavesi V, Segoni S, Rosi A, Ting X, Nery T, Catani F, Casagli N (2020) Different Approaches to Use Morphometric Attributes in Landslide Susceptibility Mapping Based on Meso-Scale Spatial Units: A Case Study in Rio de Janeiro (Brazil). Remote Sensing 12 (11), 1826. https://doi.org/10.3390/rs12111826

Carrara A, Cardinali M, Guzzetti F, Reichenbach P (1995) GIS Technology in Mapping Landslide Hazard, in: Carrara, A., Guzzetti, F. (Eds.), Geographical Information Systems in Assessing Natural Hazards. Springer Netherlands, Dordrecht, pp. 135–175. https://doi.org/10.1007/978-94-015-8404-3_8

Conoscenti C, Ciaccio M, Caraballo-Arias NA, Gómez-Gutiérrez Á, Rotigliano E, Agnesi V (2015) Assessment of susceptibility to earth-flow landslide using logistic regression and multivariate adaptive regression splines: A case of the Belice River basin (western Sicily, Italy). Geomorphology 242, 49–64. https://doi.org/10.1016/j.geomorph.2014.09.020

Conoscenti C, Sheshukov AY (2023) Regional variability of terrain index and machine learning model applications for prediction of ephemeral gullies. Geomorphology 442, 108915. https://doi.org/10.1016/j.geomorph.2023.108915

Conoscenti C, Azzara G, Sheshukov AY (2025) Pixel-scale gully erosion susceptibility: Predictive modeling with R using gully inventory consistent with terrain variables. CATENA 257, 109091. https://doi.org/10.1016/j.catena.2025.109091

Domènech G, Alvioli M, Corominas J (2020) Preparing first-time slope failures hazard maps: from pixel-based to slope unit-based. Landslides 17 (2), 249–265. https://doi.org/10.1007/s10346-019-01279-4

Felicísimo AM, Cuartero A, Remondo J, Quirós E (2013) Mapping landslide susceptibility with logistic regression, multiple adaptive regression splines, classification and regression trees, and maximum entropy methods: A comparative study. Landslides 10, 175–189. https://doi.org/10.1007/s10346-012-0320-1

Friedman JH (1991) Multivariate adaptive regression splines. The Annals of Statistics, 19(1), 1–67. https://doi.org/10.1214/aos/1176347963

Guzzetti F, Reichenbach P, Cardinali M, Galli M, Ardizzone F (2005) Probabilistic landslide hazard assessment at the basin scale. Geomorphology 72, 272–299. https://doi.org/10.1016/j.geomorph.2005.06.002

Jacobs L, Kervyn M, Reichenbach P, Rossi M, Marchesini I, Alvioli M, Dewitte O (2020) Regional susceptibility assessments with heterogeneous landslide information: Slope unit- vs. pixel-based approach. Geomorphology 356, 107084. https://doi.org/10.1016/j.geomorph.2020.107084

Kuhn M. (2008) Building predictive models in R using the caret package. Journal of Statistical Software, 28(5), 1–26. https://doi.org/10.18637/jss.v028.i05

Lindsay JB (2016) Whitebox GAT: A case study in geomorphometric analysis. Computers & Geosciences, 95, 75–84. https://doi.org/10.1016/j.cageo.2016.07.003

Martinello C, Cappadonia C, Conoscenti C, Agnesi V, Rotigliano E (2021) Optimal slope units partitioning in landslide susceptibility mapping. Journal of Maps 17 (3), 152–162. https://doi.org/10.1080/17445647.2020.1805807

Martinello C, Cappadonia C, Conoscenti C, Rotigliano E (2022a) Landform classification: a high-performing mapping unit partitioning tool for landslide susceptibility assessment—a test in the

462 Imera River basin (northern Sicily, Italy). Landslides 19 (3), 539–553.
463 https://doi.org/10.1007/s10346-021-01781-8

464 Martinello C, Mercurio C, Cappadonia C, Hernández Martínez MÁ, Reyes Martínez ME, Rivera
465 Ayala JY, Conoscenti C, Rotigliano E (2022b) Investigating Limits in Exploiting Assembled
466 Landslide Inventories for Calibrating Regional Susceptibility Models: A Test in Volcanic Areas of
467 El Salvador. Applied Sciences 12, 6151. https://doi.org/10.3390/app12126151

468 Martinello C, Cappadonia C, Rotigliano E (2023) Investigating the Effects of Cell Size in Statistical
469 Landslide Susceptibility Modelling for Different Landslide Typologies: A Test in Central–Northern
470 Sicily. Applied Sciences, 13, 1145. https://doi.org/10.3390/app13021145

471 Mercurio C, Martinello C, Rotigliano E, Argueta-Platero AA, Reyes-Martínez ME, Rivera-Ayala
472 JY, Conoscenti C (2021) Mapping Susceptibility to Debris Flows Triggered by Tropical Storms: A
473 Case Study of the San Vicente Volcano Area (El Salvador, CA). Earth 2, 66–85.
474 https://doi.org/10.3390/earth2010005

475 O'Callaghan JF, Mark DM (1984) The extraction of drainage networks from digital elevation data.
476 Computer Vision, Graphics and Image Processing, 28:323-344. https://doi.org/10.1016/S0734-
477 189X(84)80011-0

478 R Core Team (2023). R: A language and environment for statistical computing. R Foundation for
479 Statistical Computing, Vienna, Austria. URL:https://www.R-project.org/ (accessed 07 March 2026)

480 Reichenbach P, Rossi M, Malamud BD, Mihir M, Guzzetti F (2018) A review of statistically-based
481 landslide susceptibility models. Earth-Science Reviews 180, 60–91.
482 https://doi.org/10.1016/j.earscirev.2018.03.001

483 Rolain S, Alvioli M, Nguyen QD, Nguyen TL, Jacobs L, Kervyn M (2023) Influence of landslide
484 inventory timespan and data selection on slope unit-based susceptibility models. Natural Hazards
485 118 (3), 2227–2244. https://doi.org/10.1007/s11069-023-06092-w

486 Rossi M, Guzzetti F, Reichenbach P, Mondini AC, Peruccacci S (2010) Optimal landslide
487 susceptibility zonation based on multiple forecasts. Geomorphology 114, 129–142.
488 https://doi.org/10.1016/j.geomorph.2009.06.020

489 Rotigliano E, Martinello C, Agnesi V, Conoscenti C (2018) Evaluation of debris flow susceptibility
490 in El Salvador (CA): a comparison between Multivariate Adaptive Regression Splines (MARS) and
491 Binary Logistic Regression (BLR). Hungarian Geographical Bulletin 67 (4), 361–373.
492 https://doi.org/10.15201/HUNGEOBULL.67.4.5

493 Rotigliano E, Martinello C, Hernandéz MA, Agnesi V, Conoscenti C (2019) Predicting the
494 landslides triggered by the 2009 96E/Ida tropical storms in the Ilopango caldera area (El Salvador,
495 CA): optimizing MARS-based model building and validation strategies. Environmental Earth
496 Sciences 78, 210. https://doi.org/10.1007/s12665-019-8214-3

497 Van Den Eeckhaut M, Reichenbach P, Guzzetti F, Rossi M, Poesen J (2009) Combined landslide
498 inventory and susceptibility assessment based on different mapping units: an example from the
499 Flemish Ardennes, Belgium. Nat. Hazards Earth Syst. Sci. 9, 507–521.
500 https://doi.org/10.5194/nhess-9-507-2009

501 Vargas-Cuervo G, Rotigliano E, Conoscenti C (2019) Prediction of debris-avalanches and -flows
502 triggered by a tropical storm by using a stochastic approach: An application to the events occurred
503 in Mocoa (Colombia) on 1 April 2017. Geomorphology 339, 31–43.
504 https://doi.org/10.1016/j.geomorph.2019.04.023

505 Vorpahl P, Elsenbeer H, Märker M, Schröder B (2012) How can statistical models help to
506 determine driving factors of landslides? Ecological Modelling 239, 27–39.
507 https://doi.org/10.1016/j.ecolmodel.2011.12.007

508 Wang L, Liu H (2006) An efficient method for identifying and filling surface depressions in digital
509 elevation models for hydrologic analysis and modelling. International Journal of Geographical
510 Information Science, 20(2), 193–213. https://doi.org/10.1080/13658810500433453

511 Youssef AM, Pourghasemi HR, Pourtaghi ZS. Al-Katheeri MM (2016) Landslide susceptibility
512 mapping using random forest, boosted regression tree, classification and regression tree, and
513 generalized linear models and comparison of their performance at Wadi Tayyah Basin, Asir Region,
514 Saudi Arabia. Landslides 13, 839–856. https://doi.org/10.1007/s10346-015-0614-1

515